In a book "Tsunami and Nonlinear Waves": Numerical Verification of the Hasselmann equation.

Alexander O. Korotkevich[1], Andrei N. Pushkarev[2,3], Don Resio[4], and Vladimir E. Zakharov[5,2,1,3]

[1] Landau Institute for Theoretical Physics RAS, 2, Kosygin Str., Moscow, 119334, Russian Federation kao@landau.ac.ru
[2] Lebedev Physical Institute RAS,53, Leninsky Prosp., GSP-1 Moscow, 119991, Russian Federation
[3] Waves and Solitons LLC, 918 W. Windsong Dr., Phoenix, AZ 85045, USA andrei@cox.net
[4] Coastal and Hydraulics Laboratory, U.S. Army Engineer Research and Development Center, Halls Ferry Rd., Vicksburg, MS 39180, USA
[5] Department of Mathematics, University of Arizona, Tucson, AZ 85721, USA zakharov@math.arizona.edu

Summary. The purpose of this article is numerical verification of the thory of weak turbulence. We performed numerical simulation of an ensemble of nonlinearly interacting free gravity waves (swell) by two different methods: solution of primordial dynamical equations describing potential flow of the ideal fluid with a free surface and, solution of the kinetic Hasselmann equation, describing the wave ensemble in the framework of the theory of weak turbulence. Comparison of the results demonstrates pretty good applicability of the weak turbulent approach. In both cases we observed effects predicted by this theory: frequency downshift, angular spreading as well as formation of Zakharov-Filonenko spectrum $I_\omega \sim \omega^{-4}$. To achieve quantitative coincidence of the results obtained by different methods one has to accomplish the Hasselmann kinetic equation by an empirical dissipation term S_{diss} modeling the coherent effects of white-capping. Adding of the standard dissipation terms used in the industrial wave predicting model (WAM) leads to significant improvement but not resolve the discrepancy completely, leaving the question about optimal choice of S_{diss} open.

Numerical modeling of swell evolution in the framework of the dynamical equations is affected by the side effect of resonances sparsity taking place due to finite size of the modeling domain. We mostly overcame this effect using fine integration grid of 512×4096 modes. The initial spectrum peak was located at the wave number $k = 300$. Similar conditions can be hardly realized in the laboratory wave tanks. One of the results of our article consists in the fact that physical processes in finite size laboratory wave tanks and in the ocean are quite different, and the results of such laboratory experiments can be applied to modeling of the ocean phenomena

with extra care. We also present the estimate on the minimum size of the laboratory installation, allowing to model open ocean surface wave dynamics.

1 Introduction.

The theory of weak turbulence is designed for statistical description of weakly-nonlinear wave ensembles in dispersive media. The main tool of weak turbulence is kinetic equation for squared wave amplitudes, or a system of such equations. Since the discovery of the kinetic equation for bosons by Nordheim [1] (see also paper by Peierls [2]) in the context of solid state physics, this quantum-mechanical tool was applied to wide variety of classical problems, including wave turbulence in hydrodynamics, plasmas, liquid helium, nonlinear optics, etc. (see monograph by Zakharov, Falkovich and L'vov [3]). Such kinetic equations have rich families of exact solutions describing weak-turbulent Kolmogorov spectra. Also, kinetic equations for waves have self-similar solutions describing temporal or spatial evolution of weak – turbulent spectra.

However, the most remarkable example of weak turbulence is wind-driven sea. The kinetic equation describing statistically the gravity waves on the surface of ideal liquid was derived by Hasselmann [4]. Since this time the Hasselmann equation is widely used in physical oceanography as foundation for development of wave-prediction models: *WAM, SWAN* and *WAVEWATCH* – it is quite special case between other applications of the theory of weak turbulence due to the strength of industrial impact.

In spite of tremendous popularity of the Hasselmann equation, its validity and applicability for description of real wind-driven sea has never been completely proven. It was criticized by many respected authors, not only in the context of oceanography. There are at least two reasons why the weak–turbulent theory could fail, or at least be incomplete.

The first reason is presence of the coherent structures. The weak-turbulent theory describes only weakly-nonlinear resonant processes. Such processes are spatially extended, they provide weak phase and amplitude correlation on the distances significantly exceeding the wave length. However, nonlinearity also causes another phenomena, much stronger localized in space. Such phenomena – solitons, quasi-solitons and wave collapses are strongly nonlinear and cannot be described by the kinetic equations. Meanwhile, they could compete with weakly-nonlinear resonant processes and make comparable or even dominating contribution in the energy, momentum and wave-action balance. For gravity waves on the fluid surface the most important coherent structures are white-cappings (or wave-breakings), responsible for essential dissipation of wave energy.

The second reason limiting the applicability of the weak-turbulent theory is finite size of any real physical system. The kinetic equations are derived only for infinite media, where the wave vector runs continuous D-dimensional

Fourier space. Situation is different for the wave systems with boundaries, e.g. boxes with periodical or reflective boundary conditions. The Fourier space of such systems is infinite lattice of discrete eigen-modes. If the spacing of the lattice is not small enough, or the level of Fourier modes is not big enough, the whole physics of nonlinear interaction becomes completely different from the continuous case.

For these two reasons verification of the weak turbulent theory is an urgent problem, important for the whole physics of nonlinear waves. The verification can be done by direct numerical simulation of the primitive dynamical equations describing wave turbulence in nonlinear medium.

So far,the numerical experimentalists tried to check some predictions of the weak-turbulent theory, such as weak-turbulent Kolmogorov spectra. For the gravity wave turbulence the most important is Zakharov-Filonenko spectrum $F_\omega \sim \omega^{-4}$ [5]. At the moment, this spectrum was observed in numerous numerical experiments [6]- [19].

The attempts of verification of weak turbulent theory through numerical simulation of primordial dynamical equations has been started with numerical simulation of 2D optical turbulence [20], which demonstrated, in particular, co–existence of weak – turbulent and coherent events.

Numerical simulation of 2D turbulence of capillary waves was done in [6], [7], and [8]. The main results of the simulation consisted in observation of classical regime of weak turbulence with spectrum $F_\omega \sim \omega^{-19/4}$, and discovery of non-classical regime of "frozen turbulence", characterized by absence of energy transfer from low to high wave-numbers. The classical regime of turbulence was observed on the grid of 256×256 points at relatively high levels of excitation, while the "frozen" regime was realized at lower levels of excitation, or more coarse grids. The effect of "frozen" turbulence is explained by sparsity of 3-wave resonance, both exact and approximate. The classical regime of turbulence becomes possible due to nonlinear shift of the linear frequencies caused by enhanced level of excitation. Conclusion has been made that in the reality the turbulence of waves in limited systems is practically always the mixture of classical and "frozen" regimes.

In fact, the "frozen" turbulence is close to KAM regime, when the dynamics of turbulence is close to the behavior of integrable system [8].

The first attempt to perform modeling of the system of nonlinear waves (swell on the surface of deep ocean), solving simultaneously kinetic equation and primordial dynamic equations, has been done in the article [15]. The results of this simulation again confirmed ubiquity of the weak-turbulent Zakharov-Filonenko asymptotic ω^{-4} and shown existence of the inverse cascade, but presented essentially different scenario of the spectral peak evolution. Detailed analysis shown, that even on the grids as fine as 256×2048 modes, the energy transport is realized mostly by the network of few selected modes – "oligarchs" – posed in the optimal resonant condition. This regime, transitional between weak turbulence and "frozen" turbulence, should

be typical for wave turbulence in the systems of medium size. It was called "mesoscopic turbulence". Similar type of turbulence was observed in [17], [18].

In this article we present the results of new numerical experiments on modeling of swell propagation in the framework of both dynamical and kinetic equations, using fine grid containing, corresponding to 512×4096 Fourier modes. We think that our results can be considered as first in the world literature direct verification of wave kinetic equation.

One important point should be mentioned. In our experiments we observed not only weak turbulence, but also additional nonlinear dissipation of the wave energy, which could be identified as the dissipation due to white-capping. To reach agreement with dynamic experiments, we had to accomplish the kinetic equation by a phenomenological dissipation term S_{diss}. In this article we examined dissipation terms used in the industrial wave-prediction models *WAM Cycle 3* and WAM cycle 4. Dissipation term used in *WAM Cycle 3* works fairly, while S_{diss} used in WAM Cycle 4 certainly overestimate nonlinear dissipation. This fact means that for getting better agreement between dynamic and kinetic computations, we need to take into consideration more sophisticated dissipation term.

2 Deterministic and statistic models.

In the "dynamical" part of our experiment the fluid was described by two functions of horizontal variables x, y and time t: surface elevation $\eta(x, y, t)$ and velocity potential on the surface $\psi(x, y, t)$. They satisfy the canonical equations [23]

$$\frac{\partial \eta}{\partial t} = \frac{\delta H}{\delta \psi}, \quad \frac{\partial \psi}{\partial t} = -\frac{\delta H}{\delta \eta}, \tag{1}$$

Hamiltonian H is presented by the first three terms in expansion on powers of nonlinearity $\nabla\eta$

$$\begin{aligned} H &= H_0 + H_1 + H_2 + ..., \\ H_0 &= \frac{1}{2}\int \left(g\eta^2 + \psi \hat{k} \psi\right) dxdy, \\ H_1 &= \frac{1}{2}\int \eta \left[|\nabla\psi|^2 - (\hat{k}\psi)^2\right] dxdy, \\ H_2 &= \frac{1}{2}\int \eta(\hat{k}\psi) \left[\hat{k}(\eta(\hat{k}\psi)) + \eta\nabla^2\psi\right] dxdy. \end{aligned} \tag{2}$$

Here $\hat{k}$ is the linear integral operator $\hat{k} = \sqrt{-\nabla^2}$, defined in Fourier space as

$$\hat{k}\psi_{\mathbf{r}} = \frac{1}{2\pi}\int |k|\psi_{\mathbf{k}} e^{-\mathrm{i}\mathbf{kr}} \mathrm{d}\mathbf{k}, \ |k| = \sqrt{k_x^2 + k_y^2}. \tag{3}$$

Using Hamiltonian (2) and equations (1) one can get the dynamical equations [6]:

$$\begin{aligned}\dot{\eta} &= \hat{k}\psi - (\nabla(\eta\nabla\psi)) - \hat{k}[\eta\hat{k}\psi] + \\ &+\hat{k}(\eta\hat{k}[\eta\hat{k}\psi]) + \tfrac{1}{2}\nabla^2[\eta^2\hat{k}\psi] + \\ &\tfrac{1}{2}\hat{k}[\eta^2\nabla^2\psi] + \hat{F}^{-1}[\gamma_k\eta_k], \\ \dot{\psi} &= -g\eta - \tfrac{1}{2}\left[(\nabla\psi)^2 - (\hat{k}\psi)^2\right] - \\ &-[\hat{k}\psi]\hat{k}[\eta\hat{k}\psi] - [\eta\hat{k}\psi]\nabla^2\psi + \hat{F}^{-1}[\gamma_k\psi_k].\end{aligned} \tag{4}$$

Here $\hat{F}^{-1}$ corresponds to inverse Fourier transform. We introduced artificial dissipative terms $\hat{F}^{-1}[\gamma_k\psi_k]$, corresponding to pseudo-viscous high frequency damping.

It is important to stress that we added dissipation terms in both equations. In fact, equation for $\dot{\eta}$ is just kinematic boundary condition, and adding a smoothing term to this equation has no any physical sense. Nevertheless, adding of this term is necessary for stability of the numerical scheme.

The model (1)-(4) was used in the numerical experiments [6] – [8], [12], [13], [15], [17], [18].

Introduction of the complex normal variables $a_{\mathbf{k}}$

$$a_{\mathbf{k}} = \sqrt{\frac{\omega_k}{2k}}\eta_{\mathbf{k}} + \mathrm{i}\sqrt{\frac{k}{2\omega_k}}\psi_{\mathbf{k}}, \tag{5}$$

where $\omega_k = \sqrt{gk}$, transforms equations (1) into

$$\frac{\partial a_{\mathbf{k}}}{\partial t} = -\mathrm{i}\frac{\delta H}{\delta a^*_{\mathbf{k}}}. \tag{6}$$

To proceed with statistical description of the wave ensemble, first, one should perform the canonical transformation $a_{\mathbf{k}} \to b_{\mathbf{k}}$, which excludes the cubical terms in the Hamiltonian. The details of this transformation can be found in the paper by Zakharov (1999) [24]. After the transformation the Hamiltonian takes the forms

$$\begin{gathered}H = \int \omega_{\mathbf{k}} b_{\mathbf{k}} b^*_{\mathbf{k}} + \frac{1}{4}\int T_{\mathbf{k}\mathbf{k}_1\mathbf{k}_2\mathbf{k}_3} b^*_{\mathbf{k}} b^*_{\mathbf{k}_1} b_{\mathbf{k}_2} b_{\mathbf{k}_3} \times \\ \times\delta_{\mathbf{k}+\mathbf{k}_1-\mathbf{k}_2-\mathbf{k}_3}\mathrm{d}\mathbf{k}_1\mathrm{d}\mathbf{k}_2\mathrm{d}\mathbf{k}_3.\end{gathered} \tag{7}$$

where T is a homogeneous function of the third order:

$$T(\varepsilon\mathbf{k}, \varepsilon\mathbf{k}_1, \varepsilon\mathbf{k}_2, \varepsilon\mathbf{k}_3) = \varepsilon^3 T(\mathbf{k}, \mathbf{k}_1, \mathbf{k}_2, \mathbf{k}_3). \tag{8}$$

Connection between $a_{\mathbf{k}}$ and $b_{\mathbf{k}}$ together with explicit expression for $T_{\mathbf{k}\mathbf{k}_1\mathbf{k}_2\mathbf{k}_3}$ can be found, for example, in [24].

Let us introduce the pair correlation function

$$< a_{\mathbf{k}} a^*_{\mathbf{k}'} >= gN_{\mathbf{k}}\delta(\mathbf{k} - \mathbf{k}'), \tag{9}$$

where $N_{\mathbf{k}}$ is the spectral density of the wave function. This definition of the wave action is common in oceanography.

We also introduce the correlation function for transformed normal variables

$$< b_{\mathbf{k}} b^*_{\mathbf{k}'} >= g n_{\mathbf{k}} \delta(\mathbf{k} - \mathbf{k}') \tag{10}$$

Functions $n_{\mathbf{k}}$ and $N_{\mathbf{k}}$ can be expressed through each other in terms of cumbersome power series [24]. On deep water their relative difference is of the order of μ^2 (μ is the characteristic steepness) and can be neglected (in most cases of swell evolution (or wave evolution) experimental results shows $\mu \simeq 0.1$).

Spectrum $n_{\mathbf{k}}$ satisfies Hasselmann (kinetic) equation [4]

$$\begin{aligned} &\frac{\partial n_{\mathbf{k}}}{\partial t} = S_{nl}[n] + S_{diss} + 2\gamma_k n_{\mathbf{k}}, \\ &S_{nl}[n] = 2\pi g^2 \int |T_{\mathbf{k},\mathbf{k_1},\mathbf{k_2},\mathbf{k_3}}|^2 \left(n_{\mathbf{k_1}} n_{\mathbf{k_2}} n_{\mathbf{k_3}} + \right. \\ &\left. + n_{\mathbf{k}} n_{\mathbf{k_2}} n_{\mathbf{k_3}} - n_{\mathbf{k}} n_{\mathbf{k_1}} n_{\mathbf{k_2}} - n_{\mathbf{k}} n_{\mathbf{k_1}} n_{\mathbf{k_3}}\right) \times \\ &\times \delta\left(\omega_k + \omega_{k_1} - \omega_{k_2} - \omega_{k_3}\right) \times \\ &\times \delta\left(\mathbf{k} + \mathbf{k_1} - \mathbf{k_2} - \mathbf{k_3}\right) \mathrm{d}\mathbf{k_1} \mathrm{d}\mathbf{k_2} \mathrm{d}\mathbf{k_3}. \end{aligned} \tag{11}$$

Here S_{diss} is an empiric dissipative term, corresponding to white-capping.

Stationary conservative kinetic equation

$$S_{nl} = 0 \tag{12}$$

has the rich family of Kolmogorov-type [25] exact solutions. Among them is Zakharov-Filonenko spectrum [5] for the direct cascade of energy

$$n_k \sim \frac{1}{k^4}, \tag{13}$$

and Zakharov-Zaslavsky [26], [27] spectra for the inverse cascade of wave action

$$n_k \sim \frac{1}{k^{23/6}}, \tag{14}$$

3 Deterministic Numerical Experiment.

3.1 Problem Setup

The dynamical equations (4) have been solved in the real-space domain $2\pi \times 2\pi$ on the grid 512×4096 with the gravity acceleration set to $g = 1$. The solution has been performed by the spectral code, developed in [21] and previously used in [22], [12], [13], [15]. We have to stress that in the current computations the resolution in Y-direction (long axis) is better than the resolution in X-direction by the factor of 8.

This approach is reasonable if the swell is essentially anisotropic, almost one-dimensional. This assumption will be validated by the proper choice of the initial data for computation. As the initial condition, we used the Gaussian-shaped distribution in Fourier space (see Fig. 1):

$$\begin{cases} |a_{\mathbf{k}}| = A_i \exp\left(-\frac{1}{2}\frac{|\mathbf{k}-\mathbf{k}_0|^2}{D_i^2}\right), |\mathbf{k}-\mathbf{k}_0| \le 2D_i, \\ |a_{\mathbf{k}}| = 10^{-12}, |\mathbf{k}-\mathbf{k}_0| > 2D_i, \end{cases} \\ A_i = 0.92 \times 10^{-6}, D_i = 60, \mathbf{k}_0 = (0;300), \omega_0 = \sqrt{gk_0}. \tag{15}$$

The initial phases of all harmonics were random. The average steepness of this initial condition was $\mu \simeq 0.167$.

To realize similar experiment in the laboratory wave tank, one has to to generate the waves with wave-length 300 times less than the length of the tank. The width of the tank would not be less than 1/8 of its length. The minimal wave length of the gravitational wave in absence of capillary effects can be estimated as $\lambda_{min} \simeq 3cm$. The leading wavelength should be higher by the order of magnitude $\lambda \simeq 30cm$.

In such big tank of 200×25 meters experimentators can observe the evolution of the swell until approximately $700T_0$ – still less than in our experiments. In the tanks of smaller size, the effects of discreetness the Fourier space will be dominating, and experimentalists will observe either "frozen", or "mesoscopic" wave turbulence, qualitatively different from the wave turbulence in the ocean.

To stabilize high-frequency numerical instability, the damping function has been chosen as

$$\gamma_k = \begin{cases} 0, k < k_d, \\ -\gamma(k-k_d)^2, k \ge k_d, \end{cases} \\ k_d = 1024, \gamma = 5.65 \times 10^{-3}. \tag{16}$$

The simulation was performed until $t = 336$, which is equivalent to $926T_0$, where T_0 is the period of the wave, corresponding to the maximum of the initial spectral distribution.

3.2 Zakharov-Filonenko spectra

Like in the previous papers [10], [12], [13] and [15], we observed fast formation of the spectral tail, described by Zakharov-Filonenko law for the direct cascade $n_k \sim k^{-4}$ [5] (see Fig.2). In the agreement with [15], the spectral maximum slowly down-shifts to the large scales region, which corresponds to the inverse cascade [26], [27].

Also, the direct measurement of energy spectrum has been performed during the final stage of the simulation, when the spectral down shift was slow enough. This experiment can be interpreted as the ocean buoy record – the time series of the surface elevations has been recorded at one point of the surface during $T_{buoy} \simeq 300T_0$. The Fourier transform of the autocorrelation function

$$E(\omega) = \frac{1}{2\pi} \int\limits_{-T_{buoy}/2}^{T_{buoy}/2} < \eta(t+\tau)\eta(\tau) > e^{i\omega t} \mathrm{d}\tau \mathrm{d}t. \tag{17}$$

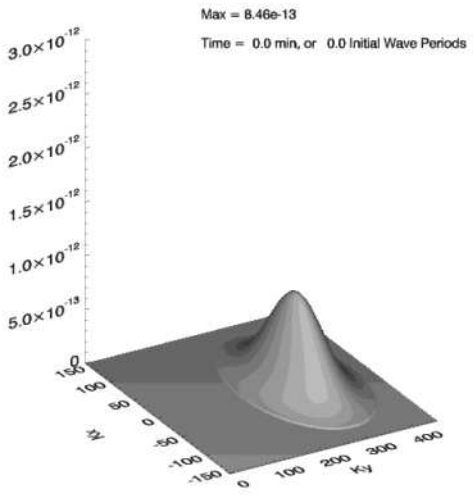

Fig. 1. Initial distribution of $|a_{\mathbf{k}}|^2$ on $\mathbf{k}$-plane.

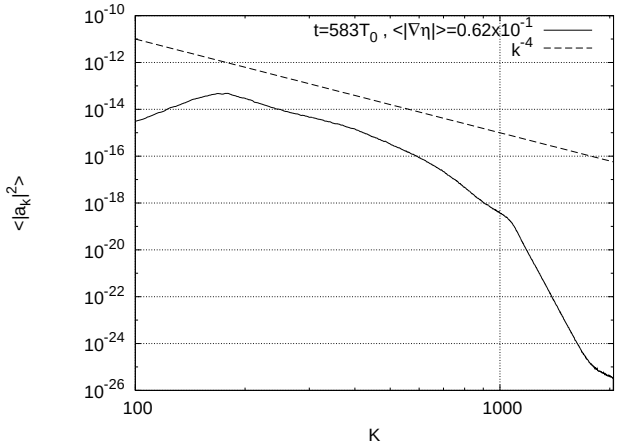

Fig. 2. Angle-averaged spectrum $n_k =< |a_{\mathbf{k}}|^2 >$ in a double logarithmic scale. The tail of distribution fits to Zakharov-Filonenko spectrum.

allows to detect the direct cascade spectrum tail proportional to ω^{-4} (see Fig.3), well known from experimental observations [28], [29], [30].

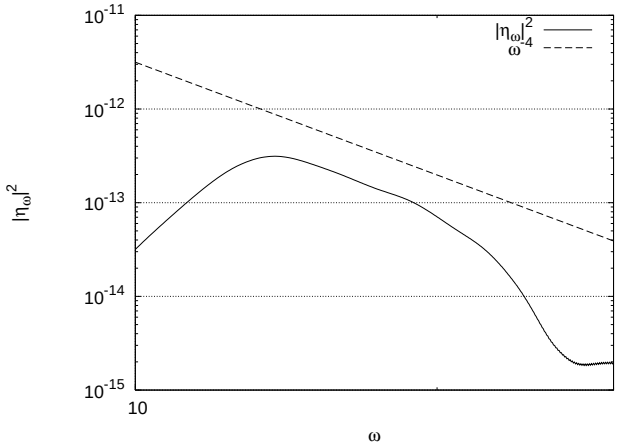

Fig. 3. Energy spectrum in a double logarithmic scale. The tail of distribution fits to asymptotics ω^{-4}.

3.3 Is the weak-turbulent scenario realized?

Presence of Kolmogorov asymptotics in spectral tails, however, is not enough to validate applicability of the weak-turbulent scenario for description of wave ensemble. We have also to be sure that statistical properties of this ensemble correspond to weak-turbulent theory assumptions.

We should stress that in our experiments at thebeginning $|a_{\mathbf{k}}|^2$ is a smooth function of $\mathbf{k}$. Only phases of individual waves are random. As shows numerical simulation, the initial condition (15) (see Fig.1) does not preserve its smoothness – it becomes rough almost immediately (see Fig.4). The picture of this roughness is remarkably preserved in many details, even as the spectrum down-shifts as a whole. This roughness does not contradict the weak-turbulent theory. According to this theory, the wave ensemble is almost Gaussian, and both real and imaginary parts of each separate harmonics are not-correlated. However, according to the weak-turbulent theory, the spectra must become smooth after averaging over long enough time of more than $1/\mu^2$ periods. Earlier we observed such restoring of smoothness in the numerical experiments of the MMT model (see [45], [46], [47] and [48]). However, in the experiments discussed in the article, the roughness still persists and the averaging does not suppresses it completely. It can be explained by sparsity of the resonances.

Resonant conditions are defined by the system of equations:

$$\begin{aligned} \omega_k + \omega_{k_1} &= \omega_{k_2} + \omega_{k_3}, \\ \mathbf{k} + \mathbf{k}_1 &= \mathbf{k}_2 + \mathbf{k}_3, \end{aligned} \tag{18}$$

These resonant conditions define five-dimensional hyper-surface in six-dimensional space $\mathbf{k}, \mathbf{k}_1, \mathbf{k}_2$. In any finite system, (18) turns into Diophantine equation.

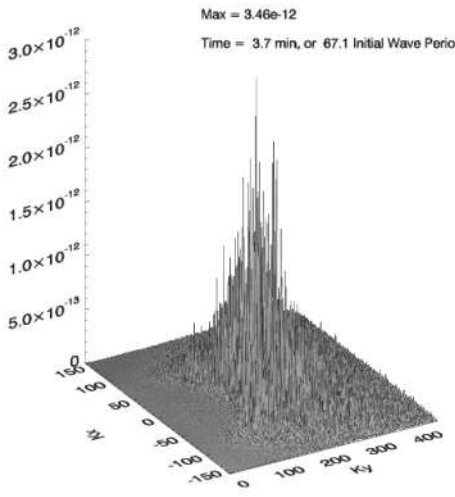

Fig. 4. Surface $|a_{\mathbf{k}}|^2$ at the moment of time $t \simeq 67T_0$.

Some solutions of this equation are known [31], [17]. In reality, however, the energy transport is realized not by exact, but "approximate" resonances, posed in a layer near the resonant surface and defined by

$$|\omega_k + \omega_{k_1} - \omega_{k_2} - \omega_{k+k_1-k_2}| \leq \Gamma, \tag{19}$$

where Γ is a characteristic inverse time of nonlinear interaction.

In the finite systems $\mathbf{k}, \mathbf{k}_1, \mathbf{k}_2$ take values on the nodes of the discrete grid. The weak turbulent approach is valid, if the density of discrete approximate resonances inside the layer (19) is high enough. In our case the lattice constant is $\Delta k = 1$, and typical relative deviation from the resonance surface

$$\frac{\Delta\omega}{\omega} \simeq \frac{\omega_k'}{\omega}\Delta k = \frac{\omega_k'}{\omega} \simeq \frac{1}{600} \simeq 2 \times 10^{-3}. \tag{20}$$

Inverse time of the interaction Γ can be estimated from our numerical experiments: wave amplitudes change essentially during 30 periods, and one can assume: $\Gamma/\omega \simeq 10^{-2} \gg \frac{\delta\omega}{\omega}$. It means that the condition for the applicability of weak turbulent theory is typically satisfied, but the "reserve" for their validity is rather modest. As a result, some particular harmonics, posed in certain "privileged" point of k-plane could form a "network" of almost resonant quadruplets and realize significant part of energy transport. Amplitudes of these harmonics exceed the average level essentially. This effect was described in the article [15], where such "selected few" harmonics were called "oligarchs". If "oligarchs" realize most part of the energy flux, the turbulence is "mesoscopic", not weak.

3.4 Statistics of the harmonics

According to the weak-turbulent scenario, statistics of the $a_{\mathbf{k}}(t)$ in any given k should be close to Gaussian. It presumes that the PDF for the squared amplitudes is

$$P(|a_{\mathbf{k}}|^2) \simeq \frac{1}{D} e^{-|a_{\mathbf{k}}|^2/D}, \tag{21}$$

here $D =< |a_{\mathbf{k}}|^2 >$ — mean square amplitude. To check equation (21) we need to find a way for calculation of $D(\mathbf{k})$. If the ensemble is stationary in time, $D(\mathbf{k})$ could be found for any given k by averaging in time. In our case, the process is non-stationary, and we have a problem with determination of $D(\mathbf{k})$.

To resolve this problem, we used low-pass filtering instead of time averaging. The low-pass filter was chosen in the form

$$f(\mathbf{n}) = e^{-(|\mathbf{n}|/\Delta)^3}, \Delta = 0.25Nx/2, Nx = 4096. \tag{22}$$

This choice of the low-pass filter preserves the values of total energy, wave action and the total momentum within three percent accuracy, see Fig.5. Then

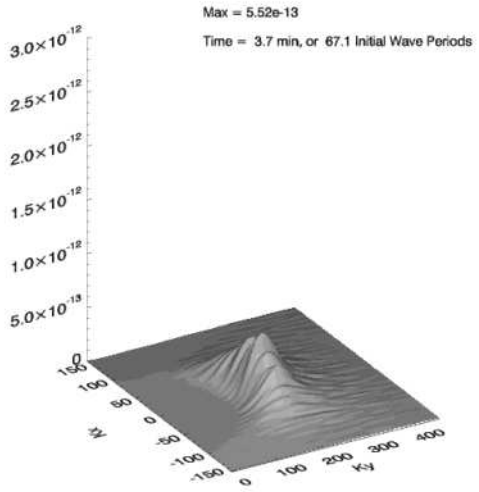

Fig. 5. Low-pass filtered surface $|a_{\mathbf{k}}|^2$ at $t \simeq 67T_0$.

it is possible to average the PDF over different areas in k-space. The results for two different moments of time $t \simeq 70T_0$ and $t \simeq 933T_0$ are presented in Fig.6 and Fig.7. The thin line gives PDF after averaging over dissipation region harmonics, while bold line presents averaging over the non-dissipative

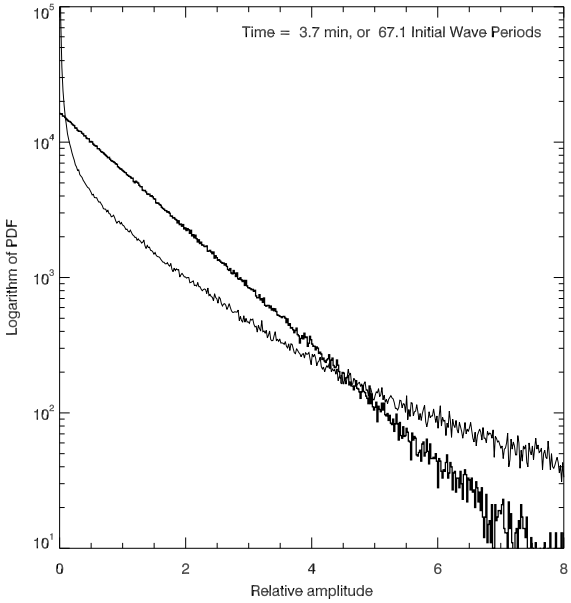

Fig. 6. Probability distribution function (PDF) for relative squared amplitudes $|a_k|^2 / < |a_k|^2 >$. $t \simeq 67T_0$.

area $|\mathbf{k}| < k_d = 1024$. One can see that statistics in the last case is quite close to the Gaussian, while in the dissipation region it deviates from Gaussian. However, deviation from the Guassianity in the dissipation region doesn't create any problems, since the "dissipative" harmonics do not contain any essential amount of the total energy, wave action and momentum.

One should remember, that the bold lines in the Fig.6 and Fig.7 are the results of averaging over a million of harmonics. Among them there is a population of "selected few", or "oligarchs", with the amplitudes exceeding the average value by the factor of more than ten times. The "oligarchs" exist because our grid is still not fine enough.

In our case "oligarchs" do exist, but their contribution in the total wave action is not more 4%. Ten leading "oligarchs" at the end of the experiment are presented in the Appendix A.

3.5 Two-stage evolution of the swell

Fig. 8-11 demonstrate time evolution of main characteristics of the wave field: wave action, energy, characteristic slope and mean frequency.

Fig.10 should be specially commented. Here and further we define the characteristic slope as follows

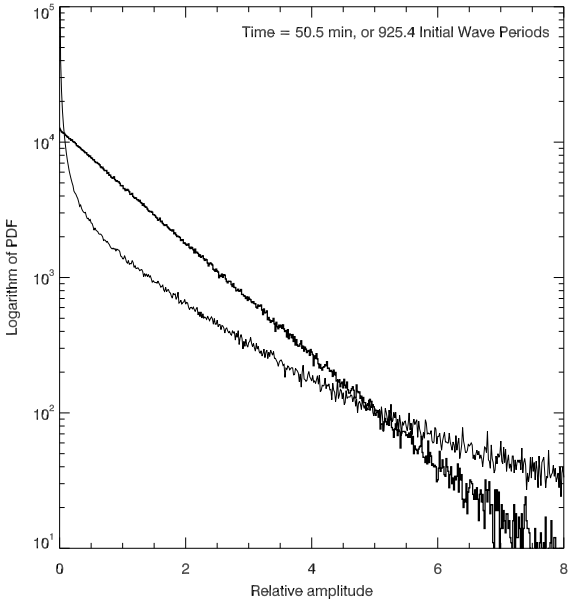

Fig. 7. Probability distribution function (PDF) for relative squared amplitudes $|a_k|^2 / < |a_k|^2 >$. $t \simeq 925 T_0$.

$$\mu = \sqrt{2} \left[< (\nabla \eta)^2 > \right]^{1/2}. \tag{23}$$

Following this definition for the Stokes wave of small amplitude

$$\eta = a \cos(kx),$$
$$\mu = ak.$$

According to this definition of steepness for the classical Pierson-Moscowitz spectrum $\mu = 0.095$. Our initial steepness $\mu \simeq 0.167$ exceeds this value essentially.

Evolution of the spectrum can be conventionally separated in two phases. On the first stage we observe fast drop of wave action, slope and especially energy. Then the drop is stabilized, and we observe slow down-shift of mean frequency together with angular spreading. Level lines of smoothed spectra in the first and in the last moments of time are shown in Fig.12-13

Presence of two stages can be explained by study of the PDFs for elevation of the surface. In the initial moment of time PDF is Gaussian (Fig.14). However, very soon intensive super-Gaussian tails appear (Fig.15). Then they decrease slowly, and in the last moment of simulation, when characteristics of the sea are close to Peirson-Moscowitz, statistic is close to Gaussian again (Fig.16). Moderate tails do exist and, what is interesting, the PDF is not

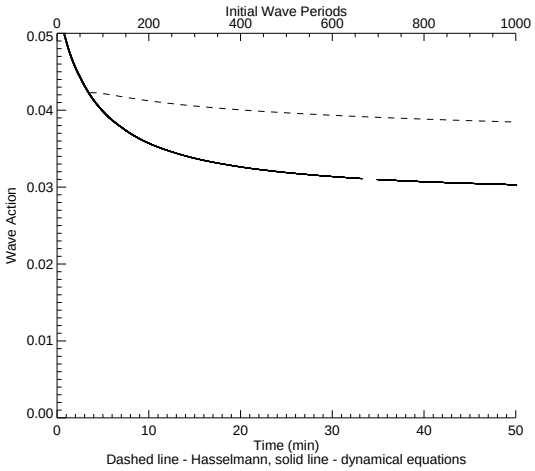

Fig. 8. Total wave action as a function of time for the artificial viscosity case.

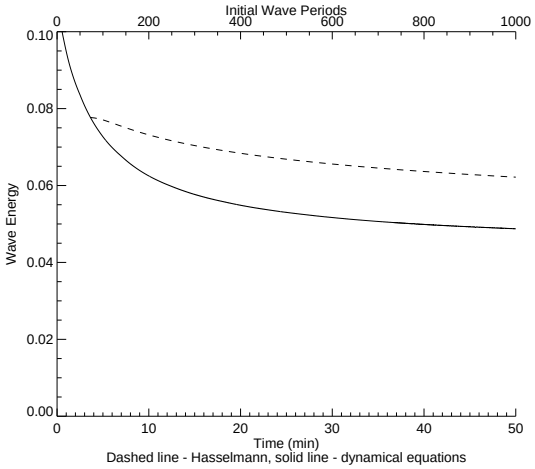

Fig. 9. Total wave energy as a function of time for the artificial viscosity case

symmetric — elevations are more probable troughs. PDF for η_y — longitudinal gradients in the first moments of time is Gaussian (Fig.17). Then in a very short period of time strong non-Gaussian tails appear and reach their maximum at $t \simeq 14T_0$ (Fig.18). Here $T_0 = 2\pi/\sqrt{k_0}$ — period of initial leading wave. Since this moment the non-Gaussian tails decrease. In the last moment of simulation they are essentially reduced(Fig.19).

Fast growing of non-Gaussian tails can be explained by fast formation of coherent harmonics. Indeed, $14T_0 \simeq 2\pi/(\omega_0\mu)$ is a characteristic time of non-

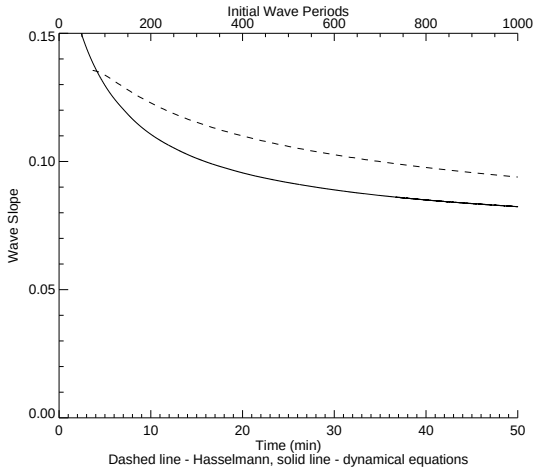

Fig. 10. Average wave slope as a function of time for the artificial viscosity case.

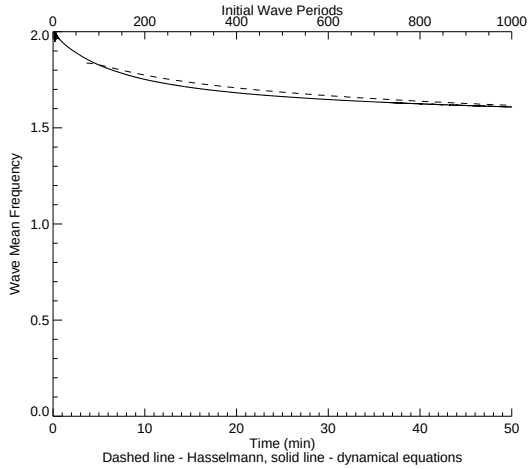

Fig. 11. Mean wave frequency as a function of time for the artificial viscosity case.

linear processes due to quadratic nonlinearity. Note that the fourth harmonic in our system is fast decaying, Hence we cannot see "real" white caps.

Figures 20-22 present PDFs for gradients in the orthogonal direction.

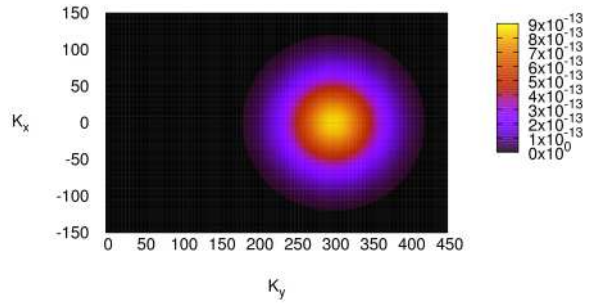

Fig. 12. Initial spectrum $|a_{\mathbf{k}}|^2$. $t = 0$.

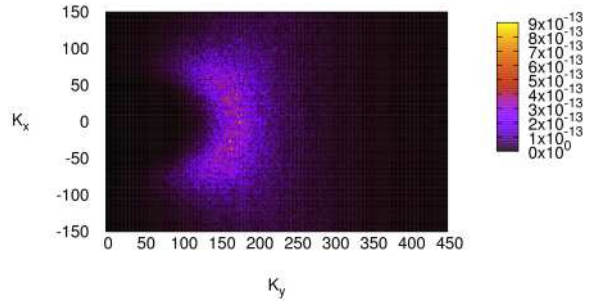

Fig. 13. Final spectrum $|a_{\mathbf{k}}|^2$. $t \simeq 933T_0$.

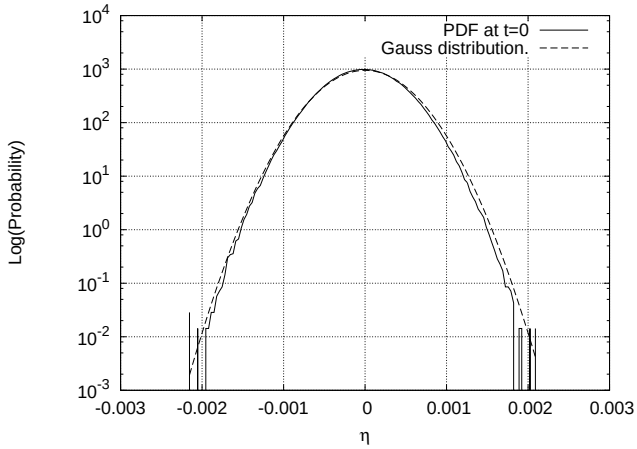

Fig. 14. PDF for the surface elevation η at the initial moment of time. $t = 0$.

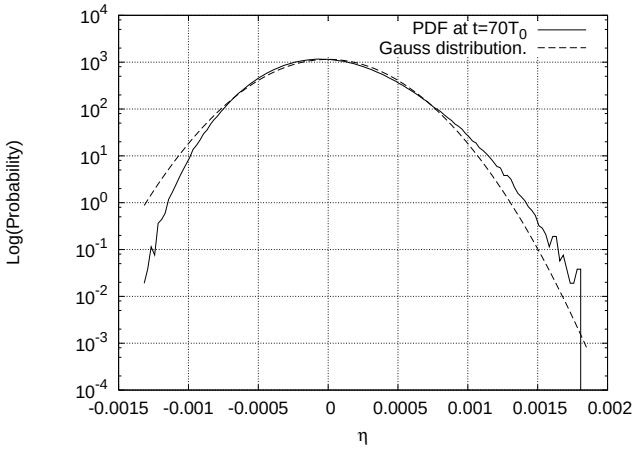

Fig. 15. PDF for the surface elevation η at some middle moment of time. $t \simeq 70T_0$.

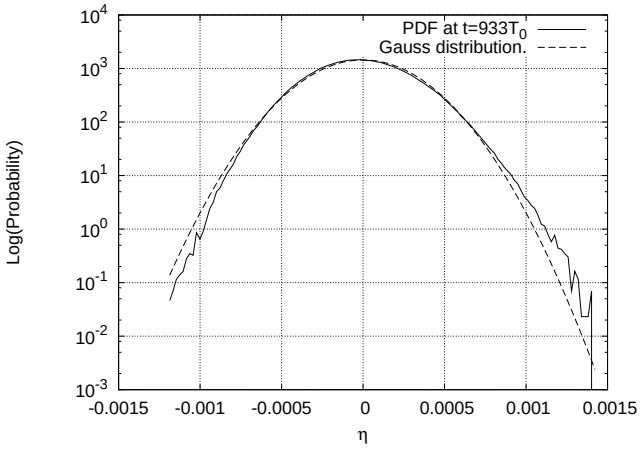

Fig. 16. PDF for the surface elevation η at the final moment of time. $t \simeq 933T_0$.

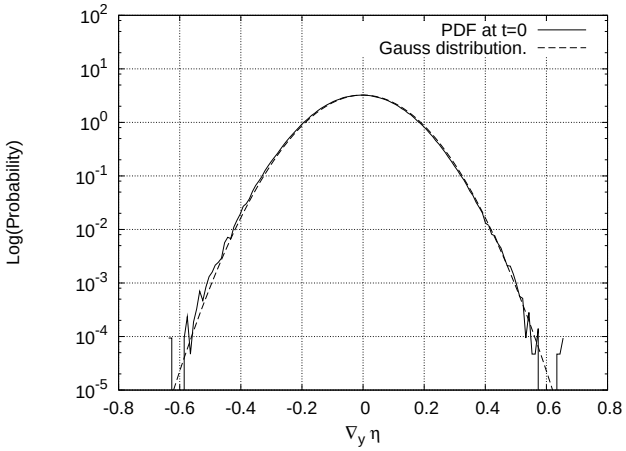

Fig. 17. PDF for $(\nabla\eta)_y$ at the initial moment of time. $t = 0$.

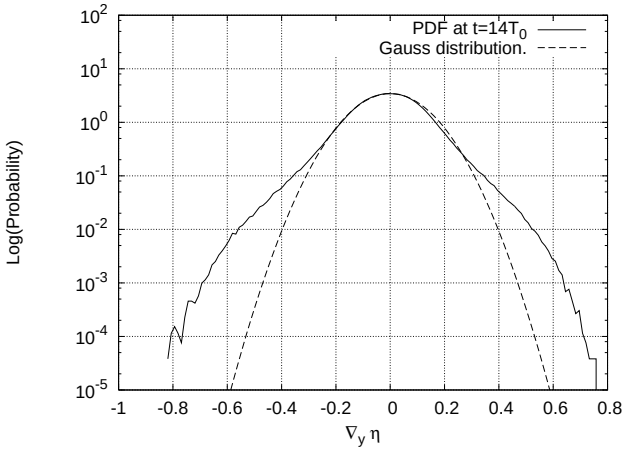

Fig. 18. PDF for $(\nabla\eta)_y$ at some middle moment of time. $t \simeq 14T_0$.

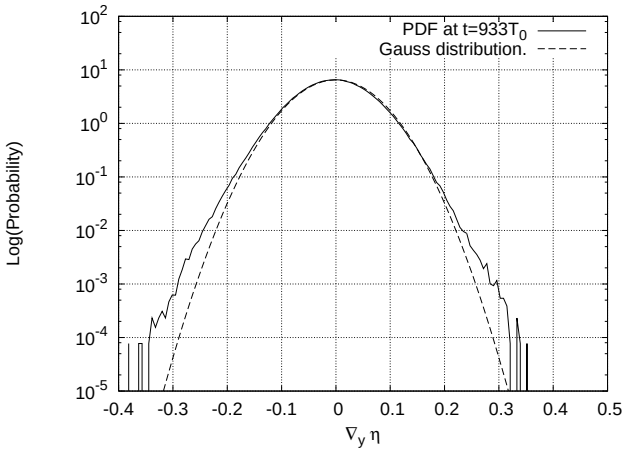

Fig. 19. PDF for $(\nabla\eta)_y$ at the final moment of time. $t \simeq 933T_0$.

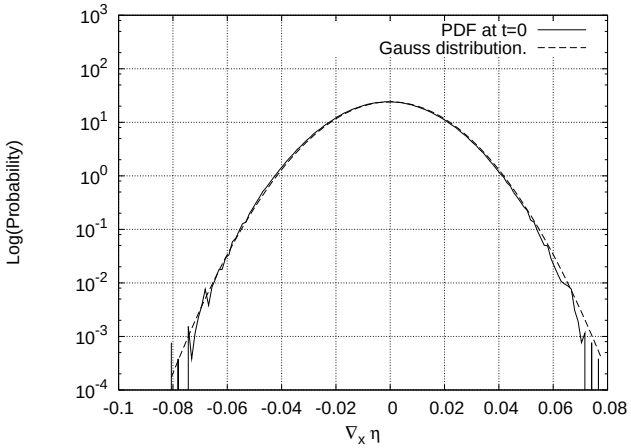

Fig. 20. PDF for $(\nabla\eta)_x$ at the initial moment of time. $t = 0$.

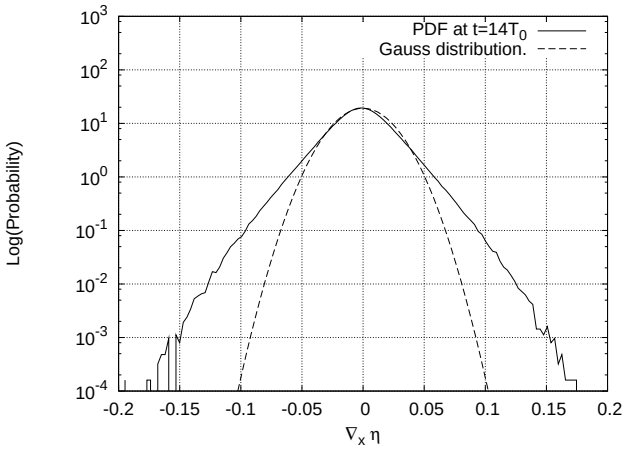

Fig. 21. PDF for $(\nabla\eta)_x$ at some middle moment of time. $t \simeq 14T_0$.

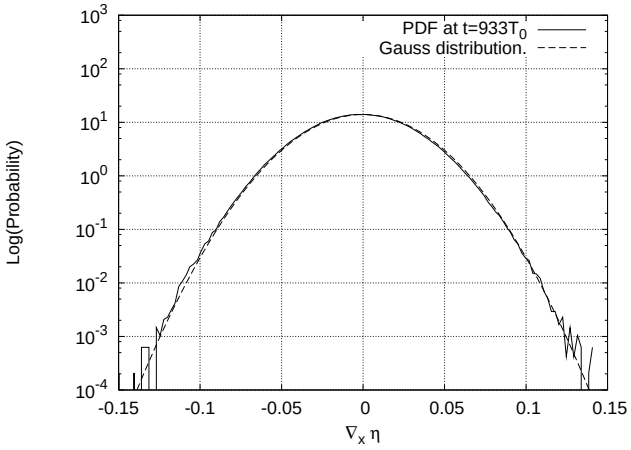

Fig. 22. PDF for $(\nabla\eta)_x$ at the final moment of time. $t \simeq 933T_0$.

Figures 23,24 present snapshots of the surface in the initial and final moments of simulation. Fig.25 is a snapshot of the surface in the moment of maximal roughness $T = 4.94 \simeq 14T_0$.

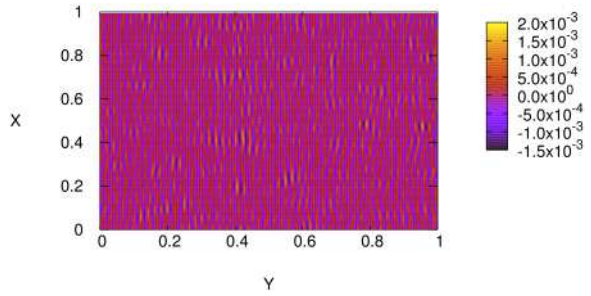

Fig. 23. Surface elevation at the initial moment of time. $t = 0$.

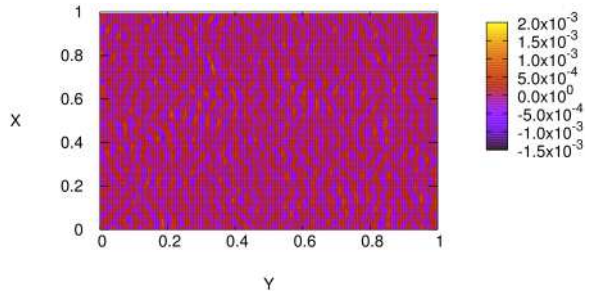

Fig. 24. Surface elevation at the final moment of time. $t \simeq 933T_0$.

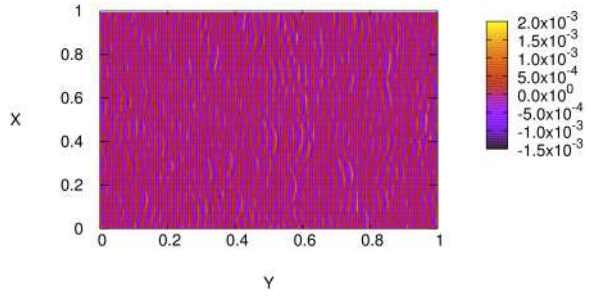

Fig. 25. Surface elevation at the moment of maximum roughness. $t \simeq 14T_0$. Gradients are more conspicuous.

4 Statistical numerical experiment

4.1 Numerical model for Hasselmann Equation

Numerical integration of kinetic equation for gravity waves on deep water (Hasselmann equation) was the subject of considerable efforts for last three decades. The "ultimate goal" of the effort – creation of the operational wave model for wave forecast based on direct solution of the Hasselmann equation – happened to be an extremely difficult computational problem due to mathematical complexity of the S_{nl} term, which requires calculation of a three-dimensional integral at every advance in time.

Historically, numerical methods of integration of kinetic equation for gravity waves exist in two "flavors".

The first one is associated with works of [32], [33], [34], [35], [36] and [37], and is based on transformation of 6-fold into 3-fold integrals using δ-functions. Such transformation leads to appearance of integrable singularities, which creates additional difficulties in calculations of the S_{nl} term.

The second type of models has been developed in works of [38] and [39], [40] and is currently known as Resio-Tracy model. It uses direct calculation of resonant quadruplet contribution into S_{nl} integral, based on the following property: given two fixed vectors $\mathbf{k}, \mathbf{k_1}$, another two $\mathbf{k_2}, \mathbf{k_3}$ are uniquely defined by the point "moving" along the resonant curve – locus.

Numerical simulation in the current work was performed with the help of modified version of the second type algorithm. Calculations were made on the grid 71×36 points in the frequency-angle domain $[\omega, \theta]$ with exponential distribution of points in the frequency domain and uniform distribution of points in the angle direction.

To date, Resio-Tracy model suffered rigorous testing and is currently used with high degree of trustworthiness: it was tested with respect to motion integrals conservation in the "clean" tests, wave action conservation in wave spectrum down-shift, realization of self – similar solution in "pure swell" and "wind forced" regimes (see [42], [41], [43]).

Description of scaling procedure from dynamical equations to Hasselman kinetic equation variables is presented in Appedix B.

4.2 Statistical model setup

The numerical model used for solution of the Hasselmann equation has been supplied with the damping term in three different forms:

1. Pseudo-viscous high frequency damping (16) used in dynamical equations;
2. $WAM1$ viscous term;
3. $WAM2$ viscous term;

Two last viscous terms referred as $WAM1$ and $WAM2$ are the "white-capping" terms, describing energy dissipation by surface waves due to white-capping, as used in $SWAN$ and WAM wave forecasting models, see [44]:

$$\gamma_{\mathbf{k}} = C_{ds}\tilde{\omega}\frac{k}{\tilde{k}}\left((1-\delta) + \ delta\frac{k}{\tilde{k}}\right)\left(\frac{\tilde{S}}{\tilde{S}_{pm}}\right)^{p} \tag{24}$$

where k and ω are wave number and frequency, tilde denotes mean value; C_{ds}, δ and p are tunable coefficients; $S = \tilde{k}\sqrt{H}$ is the overall steepness; $\tilde{S}_{PM} = (3.02 \times 10^{-3})^{1/2}$ is the value of $\tilde{S}$ for the Pierson-Moscowitz spectrum (note that the characteristic steepness $\mu = \sqrt{2}S$).

Values of tunable coefficients for $WAM1$ case (corresponding to *WAM cycle 3* dissipation) are:

$$C_{ds} = 2.36 \times 10^{-5}, \ \ \delta = 0, \ \ p = 4 \tag{25}$$

and for $WAM2$ case (corresponding to *WAM cycle 4* dissipation) are:

$$C_{ds} = 4.10 \times 10^{-5}, \ \ \delta = 0.5, \ \ p = 4 \tag{26}$$

In all three cases we used as initial data smoothed (filtered) spectra (Fig.5) obtained in the dynamical run at the time $T_* = 3.65min = 24.3 \simeq 70T_0$, which can be considered as a moment of the end of the fist "fast" stage of spectral evolution.

The natural question stemming in this point, is why calculation of the dynamical and Hasselmann model cannot be started from the initial conditions (15) simultaneously?

There are good reasons for that:

As it was mentioned before, the time evolution of the initial conditions (15) in presence of the damping term can be separated in two stages: relatively fast total energy drop in the beginning of the evolution and succeeding relatively slow total energy decrease as a function of time, see Fig.9. We explain this phenomenon by existence of the effective channel of the energy dissipation due to strong nonlinear effects, which can be associated with the white-capping.

We have started with relatively steep waves $\mu \simeq 0.167$. As we see, at that steepness white-capping is the leading effect. This fact is confirmed by numerous field and laboratory experiments. From the mathematical view-point the white-capping is formation of coherent structures – strongly correlated multiple harmonics. The spectral peak is posed in our experiments initially at $k \simeq 300$, while the edge of the damping area $k_d \simeq 1024$. Hence, only the second and the third harmonic can be developed, while hire harmonics are suppressed by the strong dissipation. Anyway, even formation of the second and the third harmonic is enough to create intensive non-Gaussian tail of the PDF for longitudinal gradients. This process is very fast. In the moment of time $T = 14T_0$ we see fully developed tails. Relatively sharp gradients mimic formation of white caps. Certainly, the "pure" Hasselmann equation is not applicable on this early stage of spectral evolution, when energy intensively dissipates.

As steepness decreases and spectral maximum of the swell down-shifts, an efficiency of such mechanism of energy absorption becomes less important

when the steepness value drops down to $\mu \simeq 0.1$the white-capping becomes a negligibly small effect. It happens at $T \simeq 280T_0$. We decided to start comparison between deterministic and statistical modeling in some intermediate moment of time $T \simeq 70T_0$.

5 Comparison of deterministic and statistical experiments.

5.1 Statistical experiment with pseudo-viscous damping term.

First simulation has been performed with pseudo-viscous damping term, equivalent to (16).

Fig.8 – 11 show total wave action, total energy, mean wave slope and mean wave frequency as the functions of time.

Fig.32 shows the time evolution of angle-averaged wave action spectra as the functions of frequency for dynamical and Hasselmann equations.

Temporal behavior of angle-averaged spectrum is presented on Fig.32. We see the down-shift of the spectral maximum both in dynamic and Hasselmann equations. The correspondence of the spectral maxima is not good at all.

It is obvious that the influence of the artificial viscosity is not strong enough to reach the correspondence of two models.

5.2 Statistical experiments with $WAM1$ damping term

Fig.33 – 36 show total wave action, total energy, mean wave slope and mean wave frequency as the functions of time.

The temporal behavior of total wave action, energy and average wave slope is much better than in the artificial viscosity term, and for $50\,min$ duration of the experiment we observe decent correspondence between dynamical and Hasselmann equations. However for longer time the $WAM1$ model deviates from the exact calculations significantly.

It is important to note that the curves of temporal behavior of the total wave action, energy and average wave slope diverge at the end of simulation time with different derivatives, and the correspondence cannot be expected to be that good outside of the simulation time interval.

Fig.37 shows the time evolution of the angle-averaged wave action spectra as the functions of frequency for dynamical and Hasselmann equations. As in the artificial viscosity case, we observe distinct down-shift of the spectral maxima. Correspondence of the time evolution of the amplitudes of the spectral maxima is much better then in artificial viscosity case.

5.3 Statistical experiments with $WAM2$ damping term

Fig.38 – 41 shows the temporal evolution of the total wave action, total energy, mean wave slope and mean wave frequency, which are divergent in time.

Fig.42 show time evolution of angle-averaged wave action spectra as the functions of frequency for dynamical and Hasselmann equations. While as in the artificial viscosity and $WAM1$ cases we also observe distinct down-shift of the spectral maxima, the correspondence of the time evolution of the amplitudes of the spectral maxima is worse than in $WAM1$ case.

Despite the fact that historically $WAM2$ appeared as an improvement of $WAM1$ damping term, it does not improve the correspondence of two models, observed in $WAM1$ case, and is presumably too strong for description of the reality.

6 Down-shift and angular spreading

The major process of time-evolution of the swell is frequency down-shift. During $T = 933T_0$ the mean frequency has been decreased from $\omega_0 = 2$ to $\omega_1 = .6$. On the last stage of the process, the mean frequency slowly decays as

$$< \omega > \simeq t^{-0.067} \simeq t^{-1/15} \tag{27}$$

The Hasselmann equation has self-similar solution, describing the evolution of the swell $n(\mathbf{k}, t) \simeq t^{4/11} F\left(\frac{\mathbf{k}}{t^{2/11}}\right)$ (see [41], [43]). For this solution

$$< \omega > \simeq t^{-1/11} \tag{28}$$

The difference between (27) and (28) can be explained as follows. What we observed, is not a self-similar behavior. Indeed, a self-silmilarity presumes that the angular structure of the solution is constant in time. Meanwhile, we observed intensive angular spreading of the initially narrow in angle, almost one-dimensional wave spectrum. Level lines of the spectra after low-pass filtering, obtained in dynamical equations simulation, for two moments of time are presented on Fig. 26-27. Level lines of the spectra in the same moments of time, obtained by solution of the Hasselmann equation are presented on Fig. 28-29. One can see good correspondance between results of both experiments. Comparison of time-evolution of the mean angular spreading calculated from action and energy spectra are presented on Fig. 30-31.

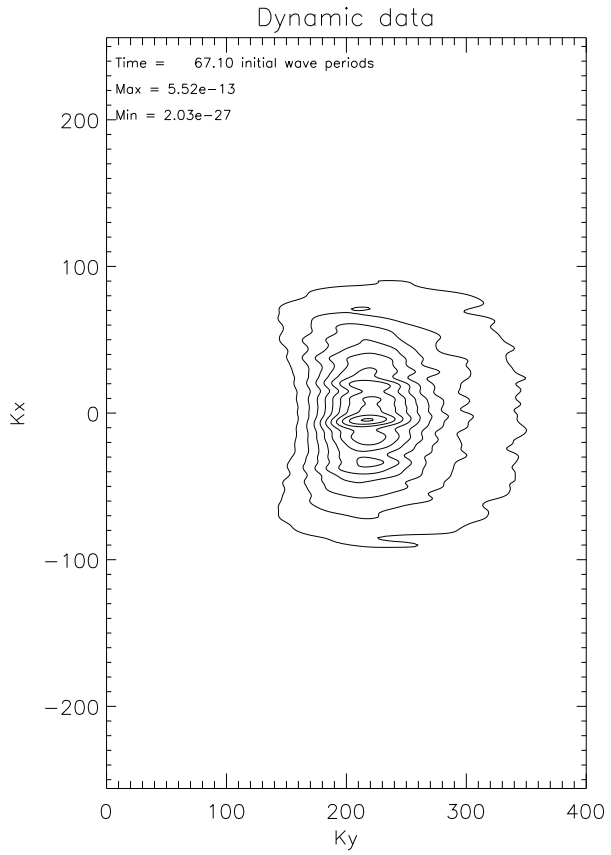

Fig. 26. Level lines of the spectra at $t = 67T_0$. Dynamical equations.

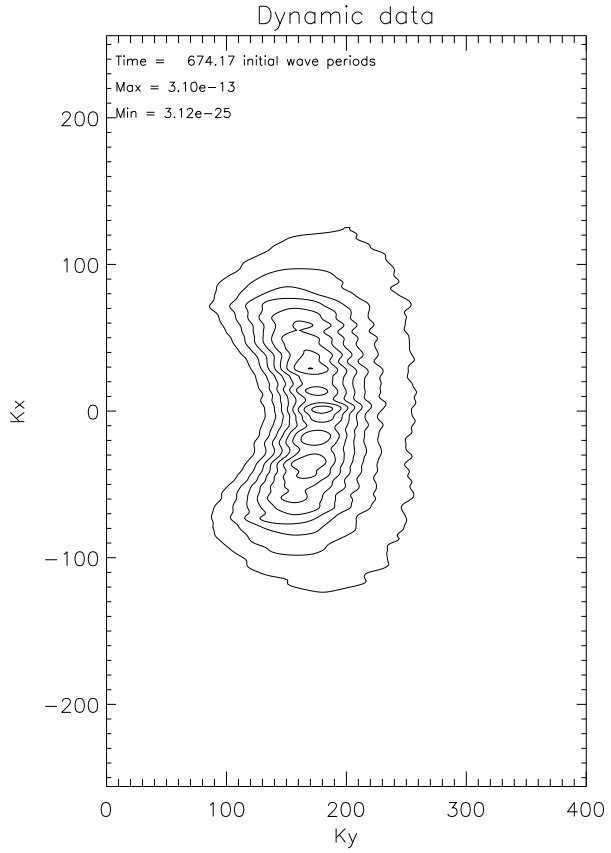

Fig. 27. Level lines of the spectra at $t = 674T_0$. Dynamical equations.

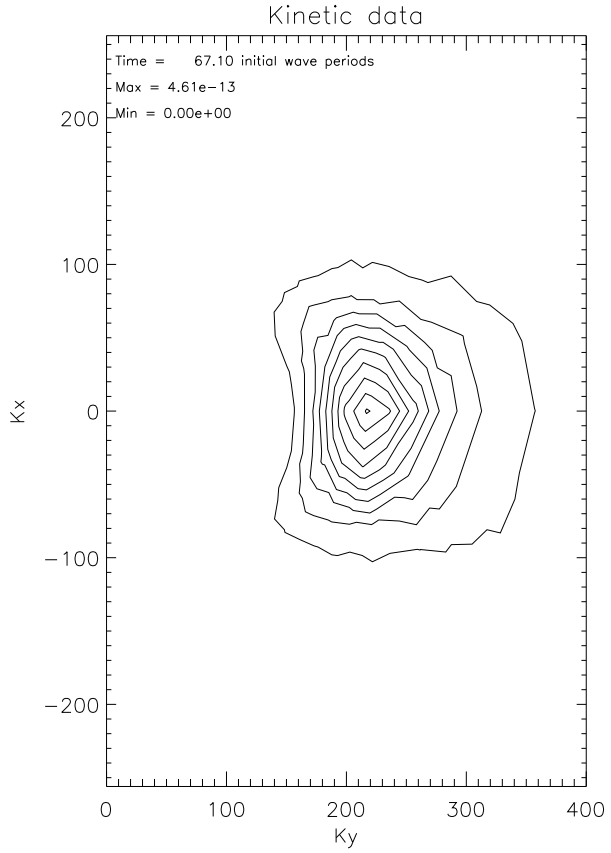

Fig. 28. Level lines of the spectra at $t = 67T_0$. Hasselmann equation.

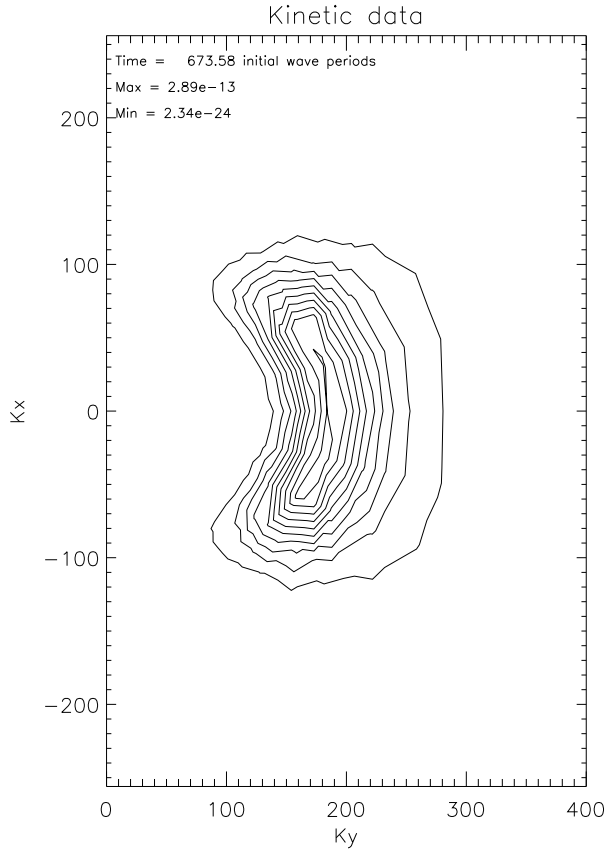

Fig. 29. Level lines of the spectra at $t = 674T_0$. Hasselmann equation.

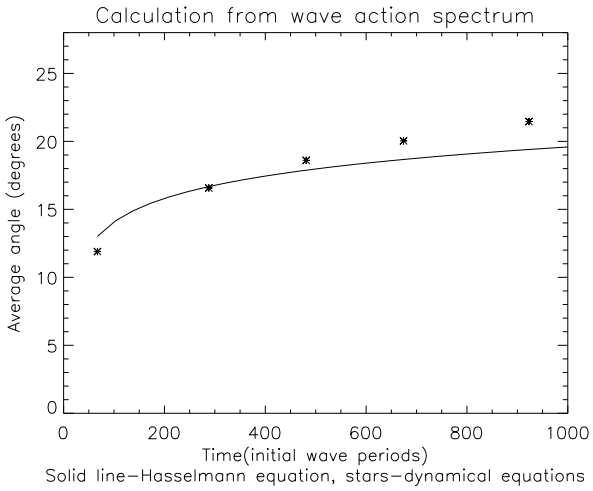

Fig. 30. Comparison of time-evolution of the mean angular spreading $\left(\int |\theta| n(\mathbf{k})\mathrm{d}\mathbf{k}\right) / \left(\int n(\mathbf{k})\mathrm{d}\mathbf{k}\right)$ calculated through wave action spectra.

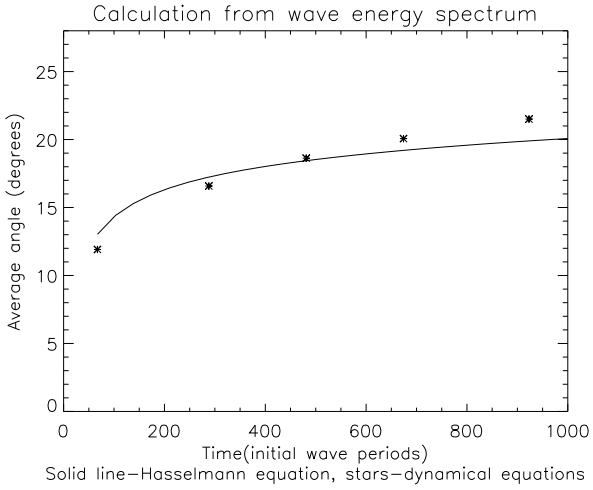

Fig. 31. Comparison of time-evolution of the mean angular spreading $\left(\int |\theta| \omega n(\mathbf{k})\mathrm{d}\mathbf{k}\right) / \left(\int \omega n(\mathbf{k})\mathrm{d}\mathbf{k}\right)$ calculated through wave energy spectra.

One has to expect that the angular spreading will be arrested at later times, and the spectra will take a universal self-similar shape.

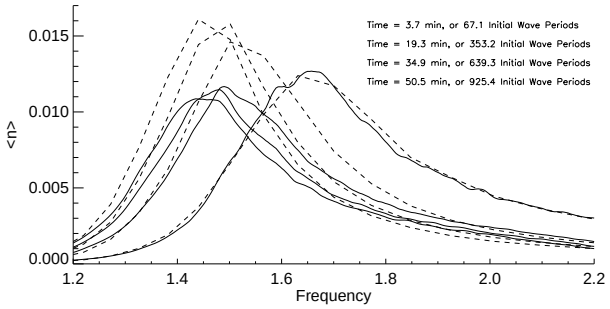

Fig. 32. Angle-averaged spectrum as a function of time for dynamical and Hasselmann equations for artificial viscosity case.

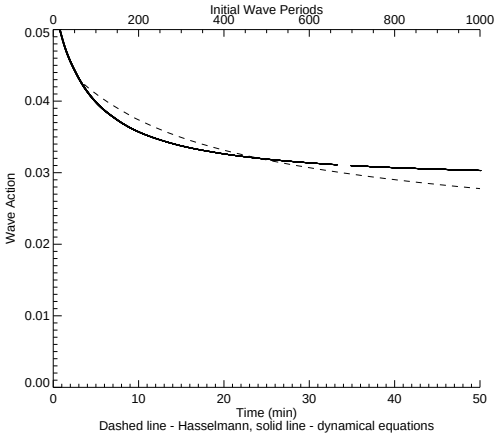

Fig. 33. Total wave action as a function of time for $WAM1$ case.

7 Conclusion

1. We started our experiment with characteristic steepness $\mu \simeq 0.167$. This is three times less than steepness of the Stokes wave of limiting amplitude,

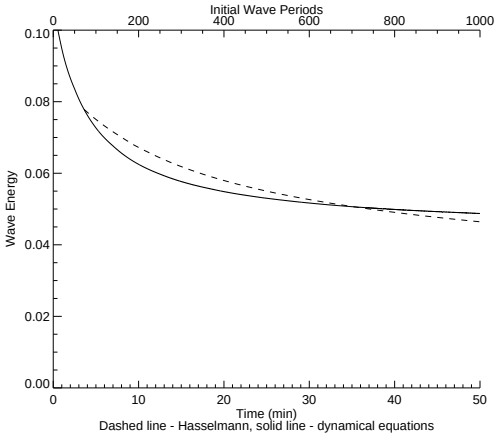

Fig. 34. Total wave energy as a function of time for $WAM1$ case

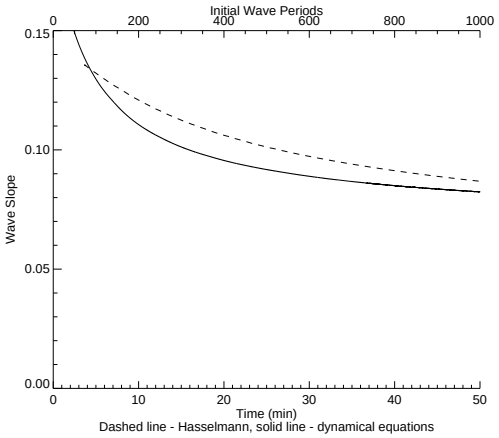

Fig. 35. Average wave slope as a function of time for $WAM1$ case.

but still it is a large steepness typical for young waves. For waves of such steepness white-capping effect could be essential. However, in our experiments we cannot observe such effects due to the strong pseudo-viscosity. Indeed, third harmonics of our initial leading wave is situated near the edge of damping area, while fourth and higher harmonics are far in the damping area. This circumstanse provides an intensive energy dissipation, which is not described by the Hasselmann equation.

Anyway, on the first stage of the process we observe intensive generation of coherent higher harmonics which reveal itself in tails of PDF for longitudinal gradients. If our damping region would be shifted further to higher wave numbers, we could observe sharp crests formation.

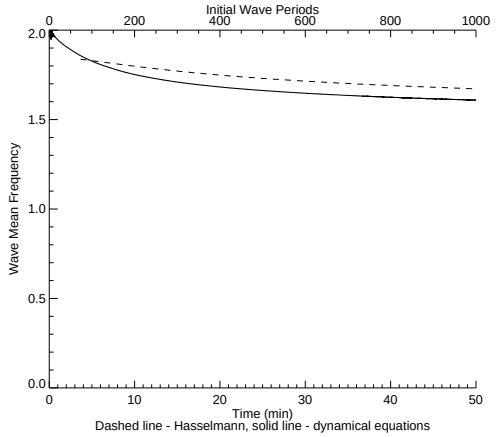

Fig. 36. Mean wave frequency as a function of time for $WAM1$ case.

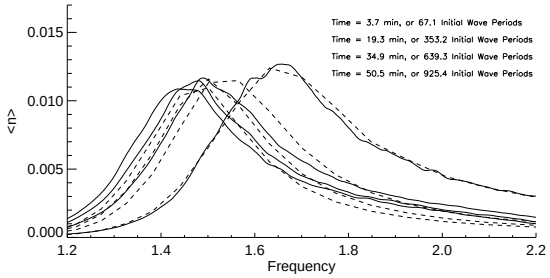

Fig. 37. Angle-averaged spectrum as a function of time for dynamical and Hasselmann equations a function of time for $WAM1$ case.

2. We ended up with steepness $\mu \simeq 0.09$. This is close to mature waves, typically observed in the ocean and described by Hasselmann equation pretty well. We observed characteristic effects predicted by the weak-turbulent theory — down-shift of mean frequency formation, Zakharov-Filonenko weak turbulent spectrum ω^{-4} and strong angular spreading. Comparison of time-derivatives of the average quantities shows that for this steepness wave-breaking (white-capping) become not essential at $\mu \simeq 0.09$.

In general, our experiments validate Hasselmann equation. However, it has to be accomplished by a proper dissipation term.

3. The dissipative term used in the $WAM1$ model fairly describe damping due to white capping on the initial stage of evolution. It overestimate damping, however, for moderate steepness $\mu \simeq 0.09$

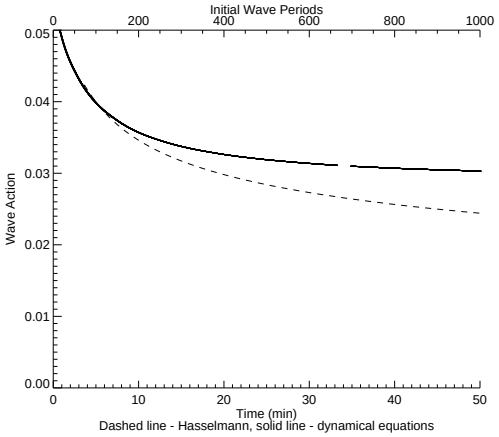

Fig. 38. Total wave action as a function of time for $WAM2$ case.

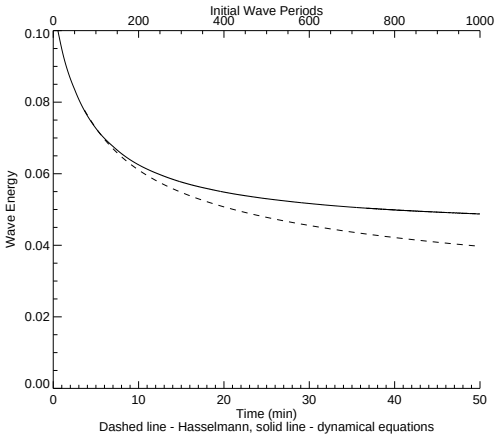

Fig. 39. Total wave energy as a function of time for $WAM2$ case

The dissipative term, used in the $WAM2$ model is not good. It overestimates damping essentially.

4. Presence of abnormally intensive harmonics, so called "oligarchs" show that, in spite of using a very fine grid, we did not eliminated effects of discreteness completely. More accurate verification of the Hasselmann equation should be made on the grid containing more than 10^7 modes. This is quite realistic task for modern supercomputers, and we hope to realize such an experiment.

Another conclusion is more pessimistic. Our results show that it is very difficult to reproduce real ocean conditions in any laboratory wave tank. Even a tank of size 200×200 meters is not large enough to model ocean due to the presence of wave numbers grid discreteness.

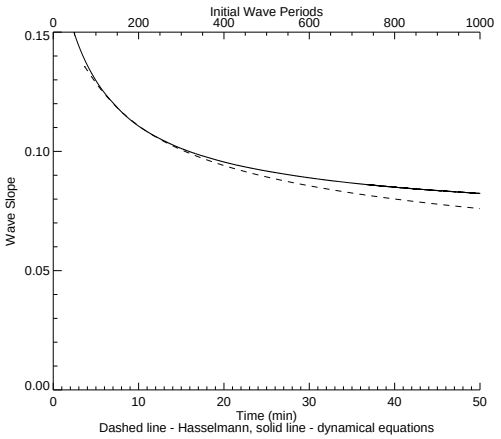

Fig. 40. Average wave slope as a function of time for $WAM2$ case.

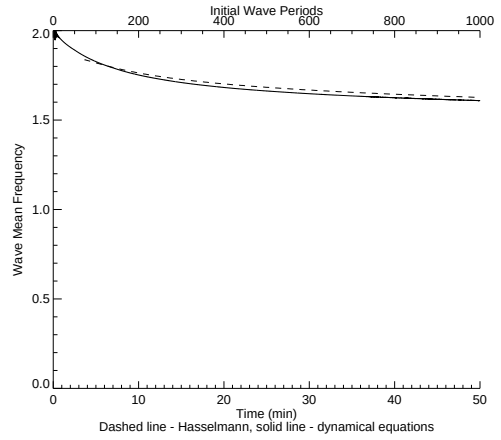

Fig. 41. Mean wave frequency as a function of time for $WAM2$ case.

8 Acknowledgments

This work was supported by ONR grant N00014-03-1-0648, RFBR grant 06-01-00665-a, INTAS grant 00-292, the Programme "Nonlinear dynamics and solitons" from the RAS Presidium and "Leading Scientific Schools of Russia" grant, also by US Army Corps of Engineers Grant DACW 42-03-C-0019 and by NSF Grant NDMS0072803.

A.O. Korotkevich was supported by Russian President grant for young scientist MK-1055.2005.2.

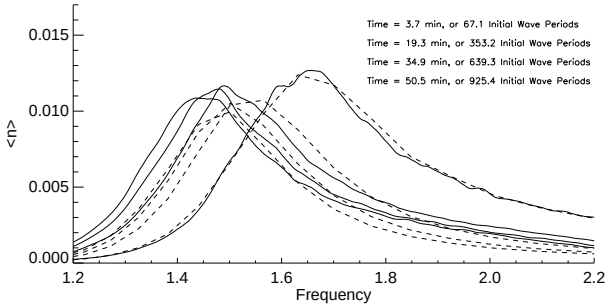

Fig. 42. Angle-averaged spectrum as a function of time for dynamical and Hasselmann equations a function of time for $WAM2$ case.

Also authors want to thank the creators of the open-source fast Fourier transform library FFTW [49] for this fast, portable and completely free piece of software.

9 Appendix A. "Forbes list of 15 largest harmonics.

Here one can find 15 largest harmonics at the end of calculations in the framework of dynamical equations. Average square of amplitudes in dissipation-less region was taken from smoothed spectrum, while all these harmonics exceed level $|a_{\mathbf{k}}|^2 = 1.4 \times 10^{-12}$.

K_x	K_y	$\|a_{\mathbf{k}}\|^2$	$<\|a_{\mathbf{k}}\|^2>_{filter}$	$\|a_{\mathbf{k}}\|^2/<\|a_{\mathbf{k}}\|^2>$
-59	155	1.563e-12	0.746e-13	2.095e+1
-37	166	1.903e-12	1.201e-13	1.585e+1
-37	185	1.569e-12	2.288e-13	0.686e+1
-36	162	1.477e-12	0.992e-13	1.489e+1
-33	157	1.442e-12	0.713e-13	2.022e+1
-26	164	3.351e-12	0.847e-13	3.956e+1
-17	189	1.463e-12	2.789e-13	0.525e+1
-14	173	1.408e-12	1.459e-13	0.965e+1
-2	176	1.533e-12	1.697e-13	0.903e+1
0	177	2.066e-12	1.741e-13	1.187e+1
10	179	1.427e-12	1.893e-13	0.754e+1
27	163	1.483e-12	0.832e-13	1.782e+1
31	174	1.431e-12	1.342e-13	1.066e+1
37	173	1.578e-12	1.581e-13	0.998e+1
60	133	1.565e-12	0.345e-13	4.536e+1

9.1 Appendix B. From Dynamical Equations to Hasselmann Equation.

Standard setup for numerical simulation of the dynamical equations (4), implies $2\pi \times 2\pi$ domain in real space and gravity acceleration $g = 1$. Usage of the domain size equal 2π is convenient because in this case wave numbers are integers.

In the contrary to dynamical equations, the kinetic equation (11) is formulated in terms of real physical variables and it is necessary to describe the transformation from the "dynamical" variables into to the "physical" ones.

Eq.4 are invariant with respect to "stretching" transformation from "dynamical" to "real" variables:

$$\eta_{\mathbf{r}} = \alpha \eta'_{\mathbf{r}'}, \quad \mathbf{k} = \frac{1}{\alpha}\mathbf{k}', \quad \mathbf{r} = \alpha \mathbf{r}', \quad g = \nu g', \tag{29}$$

$$t = \sqrt{\frac{\alpha}{\nu}} t', \quad L_x = \alpha L'_x, \quad L_y = \alpha L'_y \tag{30}$$

where prime denotes variables corresponding to dynamical equations.

In current simulation we used the stretching coefficient $\alpha = 800.00$, which allows to reformulate the statement of the problem in terms of real physics: we considered $5026\,m \times 5026\,m$ periodic boundary conditions domain of statistically uniform ocean with the same resolution in both directions and characteristic wave length of the initial condition around $22\,m$. In oceanographic terms, this statement corresponds to the "duration-limited experiment".

References

1. Nordheim LW (1928) Proc.R.Soc. A119:689
2. Peierls R (1929) Ann. Phys. (Leipzig) 3:1055
3. Zakharov VE, Falkovich G, Lvov VS (1992) Kolmogorov Spectra of Turbulence I. Springer-Verlag, Berlin
4. Hasselmann K (1962) J.Fluid Mech. 12:1
5. Zakharov VE, Filonenko NN (1966) Doklady Acad. Nauk SSSR 160:1292
6. Pushkarev AN, Zakharov VE (1996) Phys. Rev. Lett. 76:3320
7. Pushkarev AN (1999) European Journ. of Mech. B/Fluids 18:345
8. Pushkarev AN, Zakharov VE (2000) Physica D 135:98
9. Tanaka M (2001) Fluid Dyn. Res. 28:41
10. Onorato M, Osborne AR, Serio M, at al. (2002) Phys. Rev. Lett. 89:144501 arXiv:nlin.CD/0201017
11. Dysthe KB, Trulsen K, Krogstad HE, Socquet-Juglard H (2003) J. Fluid Mech. 478:1–10
12. Dyachenko AI, Korotkevich AO, Zakharov VE (2003) JETP Lett. 77:546 arXiv:physics/0308101
13. Dyachenko AI, Korotkevich AO, Zakharov VE (2004) Phys. Rev. Lett. 92:134501 arXiv:physics/0308099

14. Yokoyama N (2004) J. Fluid Mech. 501:169
15. Zakharov VE, Korotkevich AO, Pushkarev AN, Dyachenko AI (2005) JETP Lett. 82:487 arXiv:physics/0508155.
16. Dysthe K, Socquet-Juglard H, Trulsen K, at al. (2005) In "Rogue waves", Proceedings of the 14th 'Aha Huliko'a Hawaiian Winter Workshop 91:
17. Lvov Yu, Nazarenko SV, Pokorni B (2006) Physica D 218:24 arXiv:math-ph/0507054
18. Nazarenko SV (2006) J. Stat. Mech. L02002 arXiv:nlin.CD/0510054
19. Annenkov SYu, Shrira VI (2006) Phys. Rev. Lett. 96:204501
20. Dyachenko AI, Newell AC, Pushkarev AN, Zakharov VE (1992) Physica D 57:96
21. Korotkevich AO (2003) Numerical Simulation of Weak Turbulence of Surface Waves. PhD thesis, L.D. Landau Institute for Theoretical Physics RAS, Moscow, Russia
22. Dyachenko AI, Korotkevich AO, Zakharov VE (2003) JETP Lett. 77:477 arXiv:physics/0308100
23. Zakharov VE (1968) J. Appl. Mech. Tech. Phys. 2:190
24. Zakharov VE (1999) Eur. J. Mech. B/Fluids 18:327
25. Kolmogorov A (1941) Dokl. Akad. Nauk SSSR 30:9 [Proc. R. Soc. London **A434**, 9 (1991)].
26. V. E. Zakharov (1967) PhD thesis, Budker Institute for Nuclear Physics, Novosibirsk, USSR
27. Zakharov VE, Zaslavskii MM (1982) Izv. Atm. Ocean. Phys. 18:747
28. Toba Y (1973) J. Oceanogr. Soc. Jpn. 29:209
29. Donelan MA, Hamilton J, Hui WH (1985) Phil. Trans. R. Soc. London A315:509
30. Hwang PA, at al. (2000) J. Phys. Oceanogr 30:2753
31. Dyachenko AI, Zakharov VE (1994) Phys. Lett., A190:144
32. Hasselmann S, Hasselmann K, Barnett TP (1985) J. Phys. Oceanogr. 15:1378
33. Dungey JC, Hui WH (1985) Proc. R. Soc. A368:239
34. Masuda A (1981) J. Phys. Oceanogr. 10:2082
35. Masuda A (1986) in Phillips OM, Hasselmann K, Waves Dynamics and Radio Probing of the Ocean Surface. Plenum Press, New York
36. Lavrenov IV (1998) Mathematical modeling of wind waves at non-uniform ocean. Gidrometeoizdat, St.Petersburg, Russia
37. Polnikov VG (2001) Wave Motion 1008:1
38. Webb DJ (1978) Deep-Sea Res. 25:279
39. Resio D., Tracy B (1982) Theory and calculation of the nonlinear energy transfer between sea waves in deep water. Hydraulics Laboratory, US Army Engineer Waterways Experiment Station, WIS Report 11
40. Resio D, Perrie W (1991) J.Fluid Mech. 223:603
41. Pushkarev A, Resio D, Zakharov VE (2003) Physica D 184:29
42. Pushkarev A, Zakharov VE (2000) 6th International Workshop on Wave Hindcasting and Forecasting, November 6-10, Monterey, California, USA), 456 (published by Meteorological Service of Canada)
43. Badulin SI, Pushkarev A, Resio D, Zakharov VE (2005) Nonlinear Processes in Geophysics
44. SWAN Cycle III user manual, http://fluidmechanics.tudelft.nl/swan/index.htm
45. Zakharov VE, Guyenne P, Dias F (2001) Wave turbulence in one-dimensional models. Physica D, 152-153:573

46. Dias F, Pushkarev A, Zakharov VE (2004) One-Dimensional Wave Turbulence. Physics Reports, 398:1 (2004).
47. Dias F, Guyenne P, Pushkarev A, Zakharov VE (2000) Wave turbulence in one-dimensional models. Preprint N2000-4, Centre de Methematiques et del leur Appl., E.N.S de CACHAN, 1
48. Guyenne P, Zakharov VE, Dias F (2001) Turbulence of one-dimensional weakly nonlinear dispersive waves. Contemporary Mathematics, 283:107
49. Frigo M, Johnson SG (2005) Proc. IEEE 93:216 http://fftw.org.